DOI: 10.1002/ejic.200900362

Controllable Synthesis of Shuttle-Shaped Ceria and Its Catalytic Properties for CO Oxidation

Chunwen Sun*[a,b] and Liquan Chen[a]

Keywords: Nanostructures / Nanoparticles / Solvothermal synthesis / Ceria / Catalytic properties

Shuttle-shaped ceria was obtained in a high yield via a surfactant octadecylamine and urea assisted solvothermal process. The crystalline structure and morphology were characterized with powder X-ray diffraction (XRD), scanning electron microscope (SEM), and transmission electron microscope (TEM). Preliminary catalytic measurement shows that the shuttle-shaped CeO_2 exhibits an enhanced activity for CO oxidation, which may be attributed to its higher porosity and more oxygen vacancies.

Introduction

In recent years, great efforts have been made to synthesize shape- and size-controlled metal oxides with unique properties due to their fundamental scientific interest and potential technological applications.[1] Ceria (CeO_2) plays a vital role in emerging technologies for environmental and energy related applications. It is widely used as a promoter in three-way catalysts (TWC) for the elimination of toxic auto-exhaust gases,[2] low-temperature water-gas shift reaction,[3] fuel cells,[4] oxygen sensors[5] and oxygen permeation membrane systems.[6] Nanocrystalline CeO_2 has showed improved and size-dependent properties.[7] Up to now, various nanostructured ceria have been synthesized, including nanowires,[8] nanorods,[9] nanotubes,[10] nanocubes,[11] flowerlike hollow sphere,[7b,7d] and mesoporous particles.[12] However, there are few reports on preparation of shuttle-shaped CeO_2 material.

Herein, we report for the first time the synthesis of hierarchically shuttle-shaped CeO_2 consisting of nanorods via a facile solvothermal method. The preliminary result shows that shuttle-shaped CeO_2 exhibits an enhanced catalytic activity for CO oxidation compared with that of CeO_2 nanorod sample.

Results and Discussion

Figure 1 shows the typical XRD pattern of as-prepared samples. All the peaks can be indexed to a pure phase face-centered cubic [space group: *Fm3m*(225)] of ceria (JCPDS no 34–0394). It is noticed that the width of the peaks is obviously broadened, a typical feature of nanostructured materials.

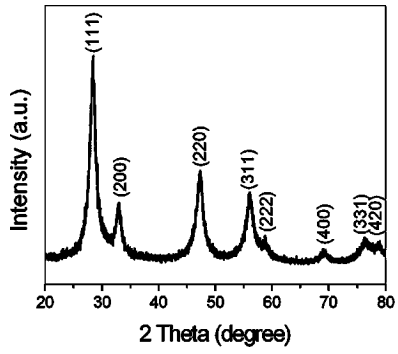

Figure 1. XRD pattern of the as-prepared sample.

Figure 2 shows typical field-emission scanning electron microscope (FESEM) images of as-prepared CeO_2. It can be seen that the particles have a shuttle-like shape. From high magnification SEM image (Figure 2, b) and TEM images (Figure 2, c), it can be seen that the shuttle-shaped particles are composed of packed nanorods. The length of nanorods is about 500–700 nm and the diameter ranges from 10 to 20 nm. Compared with well-dispersed nanorods, higher porosity and surface area are obtained due to the parallel-aligned nanorods in shuttle-shaped CeO_2. Figure 2 (d) is a high-resolution TEM (HRTEM) image of the nanorods. The interplanar spacings of the ordered strips in Figure 2 (d) are about 0.31 and 0.27 nm, which are consistent with the (111) and (200) lattice planes of CeO_2, respectively. The HRTEM image indicates clearly that the nanorod is composed of many tiny grains with different orientations (average grain size of 3–5 nm, Figure 2, d).

[a] Beijing National Laboratory for Condensed Matter Physics, Institute of Physics, Chinese Academy of Sciences,
Beijing 100080, P. R. China
[b] Institute for Fuel Cell Innovation, National Research Council Canada,
4250 Wesbrook Mall, Vancouver, BC V6T 1W5, Canada
Fax: +1-604-221-3001
E-mail: Springwensun@yahoo.com.cn

Supporting information for this article is available on the WWW under http://dx.doi.org/10.1002/ejic.200900362.

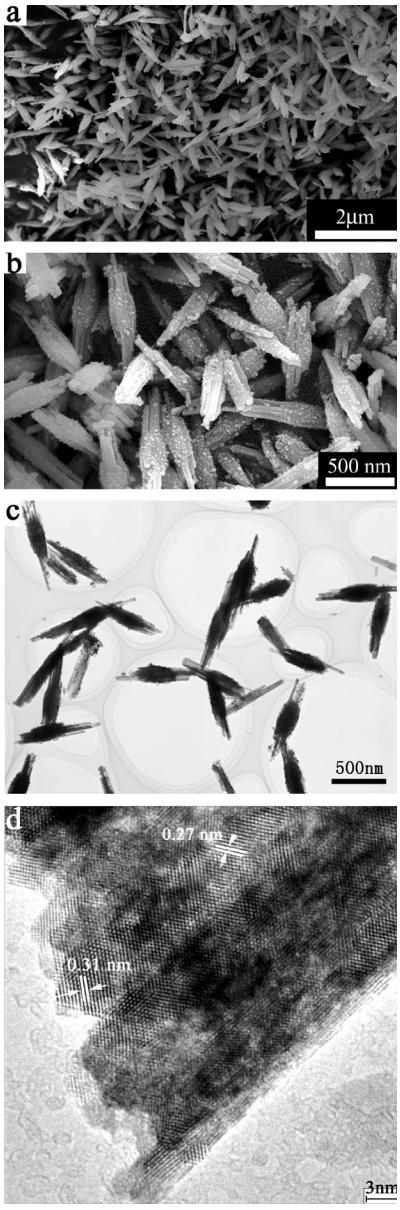

Figure 2. SEM images (a,b) and TEM images (c,d) of shuttle-shaped ceria.

The elementary composition and chemical valence on the surface of the as-prepared shuttle-shaped ceria were detected by XPS. Figure 3 (a) shows the XPS survey spectrum of the as-synthesized ceria sample. Core levels of Ce 3d, Ce 4d, C 1s, and O 1s can be identified. The spectrum of Ce 3d can be decomposed into eight components with the assignment defined in Figure 3 (b). According to the literature,[13,14] the bands v′ and u′ are the satellites arising from the Ce $3d_{5/2}$ and Ce $3d_{3/2}$ ionizations of Ce^{3+} ions. From Figure 3 (b), it can be seen that the chemical valence of cerium on the surface of shuttle-shaped ceria nanoparticles was mainly Ce^{4+} plus a small proportion of Ce^{3+}. For comparison, CeO_2 nanorod sample was also prepared according to the methods reported in the literature.[15] Compared with those of shuttle-shaped ceria, the peaks of the bands v′ and u′ in the XPS spectra of the as-prepared CeO_2 nanorods (see Figure S1 in the Supporting Information) are relatively weak. This result means there are more oxygen vacancies in this shuttle-shaped CeO_2 sample. Structure defects and oxygen vacancy usually act as promoting sites for many catalytic reaction.[2b,15,16]

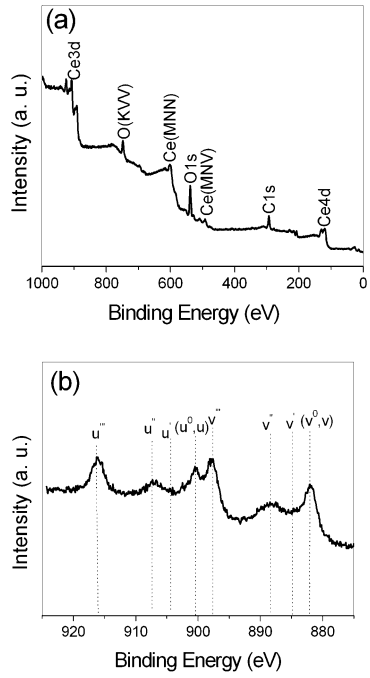

Figure 3. XPS spectra of the as-prepared ceria samples: (a) wide spectrum and (b) Ce 3d spectrum.

The thermal stability of shuttle-shaped CeO_2 was analysed by thermogravimetric analysis (TGA) and differential thermal analysis (DTA). A representative TGA-DSC profile under flowing air is shown in Figure 4. The initial weight loss from 30 °C to 150 °C is attributed to the loss of surface-adsorbed water. The weight loss in the temperature range of 150–325 °C is due to the removal of the water molecules of crystallization and remnant organic compounds. It is noted that a little of weight gain occurs at 270–300 °C, which may correspond to the conversion of three valent CeO_{2-x} into CeO_2. An endothermic peak was observed in the DSC curve at 270–320 °C due to a collectively thermal effect of the above-mentioned processes. After 320 °C, the weight loss continues but gradually slows down (Figure 5).

Nitrogen adsorption–desorption isotherms and the corresponding Barret–Joyner–Halenda (BJH) pore size distribution curve of the obtained shuttle-shaped ceria product are shown in parts a and b of Figure 4, respectively. The measured Brunauer–Emmett–Teller (BET) surface area is 83.3 $m^2 g^{-1}$ from the nitrogen adsorption–desorption isotherm. Calculated from the desorption branch of the nitrogen isotherm, the corresponding BJH desorption cumulative pore volume is 0.33 $cm^3 g^{-1}$. The average pore diameter is determined to be 18.1 nm. From Figure 4 (b) it can be seen that there is a large pore distribution with a diameter

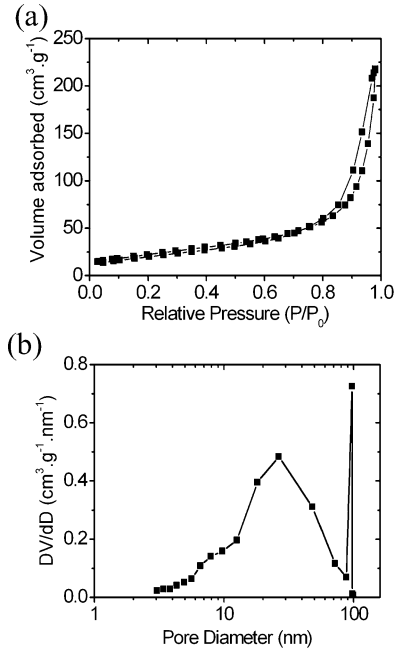

Figure 4. N_2 adsorption-desorption isotherms (a) and the corresponding BJH pore size distribution of the as-prepared shuttle-shaped ceria sample.

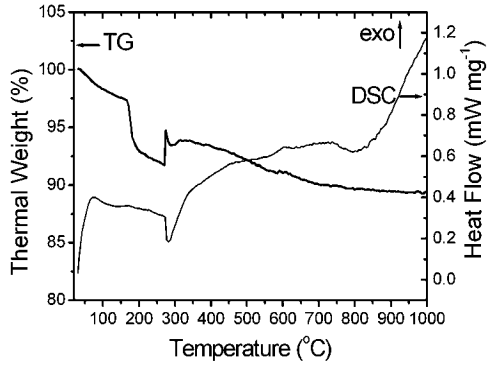

Figure 5. TG-DSC curves of the as-prepared shuttle-shaped ceria sample.

about 97 nm, which may arise from the voids between the parallel aligned nanorods. In comparison, the measured BET surface area for CeO_2 nanorods is 26.1 $m^2 g^{-1}$ (Figure S2). The cumulative pore volume is 0.09 $cm^3 g^{-1}$.

For clarifying the formation process of shuttle-shaped CeO_2 particles obtained under the typical synthetic conditions as shown in the Exp. Section (pH ≈ 2–3), we examined whether the shuttle-shaped CeO_2 can be obtained under the alkaline condition (pH = 14) or neutral condition (pH = 7) since the hydrolyzation of urea is usually varied with the pH value of reaction systems. Figure S3 (a, b) show the SEM images of samples synthesized under the same conditions except that the pH value was different. When 1 mol L^{-1} sodium hydroxide was used to adjust the pH value to 14, small rod-like particles were observed (Figure S3a). However, when nitric acid or sodium hydroxide was not used, that is, the pH value of the precursor was close to 7, only bigger bulk aggregates were observed (Figure S3b). Usually, the evolution of a solid from a solution phase involves two steps in crystallization: nucleation and growth.[17] The above experimental results indicate that the pH value is an important factor affecting the growth habit of ceria, and acidic environment is a crucial factor for the formation of shuttle-shaped nanoparticles. We also investigate the influence of urea and octadecylamine on the morphology of products. The sample was prepared under the same conditions except that urea and octadecylamine were absent, respectively. As shown in Figure S4a, the coexistence of nanorods and bulk particles was observed in the absence of urea. However, in the absence of octadecylamine, only small nanoparticles were observed (Figure S4b). This indicates that octadecylamine plays an important role as the structure-directing agent for the formation of one-dimensional (1D) nanorods, which was also confirmed in our previous study.[9c]

The effect of reaction temperature was studied by fixing other conditions and the reaction temperature was changed to 130 and 180 °C, respectively. SEM images showed that small sphere-like aggregates were obtained below 130 °C (Figure S5a). In contrast, the product prepared at 180 °C shows large irregular particles (Figure S5b). It indicates that low reaction temperature is good for the formation of small nuclei. In contrast, high temperature is beneficial for crystal growth; however, it may not good for the preferred growth along a certain direction.

During the formation process of shuttle-shaped CeO_2, we believe that urea plays a crucial role. In an aqueous solution, urea produces ammonium and cyanate ions [Equation (1)].

$$H_2N–CO–NH_2 \leftrightarrows NH_4^+ + OCN^- \quad (1)$$

It is well known that the hydrolyzation of urea is varied with the pH value of reaction systems.[18]

In neutral and basic solutions, carbonate ions and ammonia are formed [Equation (2)].

$$OCN^- + OH^- + H_2O \rightarrow NH_3 + CO_3^{2-} \quad (2)$$

Therefore, the obtained products are usually cerium carbonate hydroxide ($CeOHCO_3$).[19]

However, in an acidic solution similar to this case, cyanate ions rapidly react according to the following reaction (3).

$$OCN^- + 2H^+ + H_2O \rightarrow CO_2 + NH_4^+ \quad (3)$$

At low pH, cerium ions usually undergo strong hydration and the hydrated cerium ions can form complexes with H_2O molecules or OH^- ions according to the following reaction (4).[18]

$$[Ce(H_2O)_n]^{m+} + yH_2O \rightarrow [Ce(OH)_y(H_2O)_{n-y}]^{(m-y)+} + yH_3O^+ \quad (4)$$

In an aqueous solution, H_2O as a polar molecule tends to take protons away from the hydroxide [Equation (5)].

$$Ce(OH)_y(H_2O)_x^{(m-y)+} + H_2O \rightarrow CeO_{m/2}{\cdot}n(H_2O) + H_3O^+ \quad (5)$$

A two-step growth mechanism is proposed for the formation process of shuttle-shaped CeO_2, involving an oriented attachment of the colloidal $CeO_{m/2}{\cdot}n(H_2O)$ precipitates for decreasing the surface energy and the subsequent growth of nanoparticles directed by the surfactant octadecylamine via hydrogen bonding, van der Waals forces, and/or electrostatic interaction. Further experimental work is needed to elucidate the exact growth mechanism of shuttle-shaped CeO_2 particles.

CO oxidation reaction is an important process in three-way catalysis for the elimination of toxic auto-exhaust gases. As shown in Figure 6, it can be seen that the CO conversion over shuttle-shaped CeO_2 reaches more than 80% at 210 °C and complete CO oxidation is achieved at about 250 °C. For CeO_2 nanorod, T_{50} is about 290 °C. Higher porosity and surface area as well as more oxygen vacancies in the shuttle-shaped CeO_2 may be responsible for its higher catalytic activity for CO oxidation reaction.

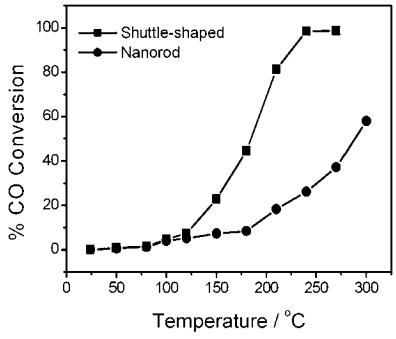

Figure 6. Catalytic activity of CO oxidation over shuttle-shaped and nanorod ceria.

Conclusions

In summary, shuttle-shaped ceria particles have been synthesized on a large scale by a solvothermal method. The shuttle-shaped particles are composed of packed nanorods, which have higher porosity, surface area and more oxygen vacancies. Preliminary catalytic measurements show that the shuttle-shaped CeO_2 exhibits an enhanced catalytic activity for CO oxidation compared with that of rod-shaped CeO_2 sample. This novel structure CeO_2 material shows great potentials as a support for catalysts with various purposes, such as low-temperature water-gas shift reaction and elimination of toxic auto-exhaust gases.

Experimental Section

Solvothermal Synthesis: All chemicals were purchased from Beijing Chemical Reagents Company and used without further purification. Under a typical synthetic condition, 0.01 mol of octadecylamine was dissolved into a solution containing 40 mL deionized water and 40 mL absolute ethanol. 0.01 mol hydrated cerium(III) nitrate and 0.05 mol urea was added in sequence under magnetic stirring after the octadecylamine was completely dissolved. After that, 4 mL of 8 mol L^{-1} nitric acid was dropped into the above solution to control pH ≈ 2–3. The mixture was stirred for three hours before being transferred into a 100 mL Teflon-lined autoclave. Then the autoclave was sealed and kept at 160 °C for 72 h. After that, the autoclave was cooled down to room temperature naturally. The supernatant liquid was discarded and the remaining product was washed with acetone, hot ethanol solution and deionized water in sequence for more than three times, then separated by centrifugation. The product was dried in a vacuum oven at 120 °C for 6 h.

Characterization: The phase structure of the as-prepared products was characterized by X-ray powder diffraction (XRD) using a Rigaku X-ray diffractometer with Cu-K_α radiation (Japan, Rigaku, D/max-RB). The microstructure and morphology of CeO_2 nanoparticles were characterized by a scanning electron microscope (SEM, XL30s-FEG, 10 kV) and a transmission electron microscope (TEM, JEOL JEM-2010, 200 kV). Before SEM experiments, the samples were coated with gold by sputtering to minimize charging effects under SEM imaging conditions. Surface composition was determined by X-ray photoelectron spectroscopy (XPS) using VG's Sigma probe system (Thermo VG Scientific, U. K.). The binding energies (BE) for samples were calibrated by setting the measured BE of C1s to 284.6 eV. To avoid the reduction of Ce^{4+} to Ce^{3+} by irradiation damage of X-ray beam on the tested sample, the collection time was within 10 min for each measurement. Thermogravimetric analysis (TGA) and differential thermal analysis (DTA) profiles were collected with a NETZSCH STA 449C high-temperature thermoanalyzer apparatus (Netzsch Inc., Germany) at a heating rate of 10 °C min^{-1} from 30 °C to 1000 °C in flowing air at a rate of 30 mL min^{-1}. The nitrogen adsorption and desorption isotherm at 77 K was measured using a NOVA4000 Surface Area & Pore Size Analyzer (Quantachrome Instruments, U.S.) after the samples were vacuum dried at 200 °C for over 10 h.

The catalytic activity for CO oxidation was evaluated in a fixed-bed quartz tubular reactor. The catalyst particles (0.15 g) were placed in the reactor. The reactant gases (1.0% CO, 19% O_2, balanced with nitrogen) went through the reactor at a rate of 100 mL min^{-1}. The composition of the gas exiting the reactor was monitored by a gas chromatogram. T_{50} is defined as the temperature at which the conversion of CO to CO_2 reaches 50%.

Supporting Information (see also the footnote on the first page of this article): XPS spectra and N_2 adsorption-desorption isotherms of the as-prepared CeO2 nanorod sample; SEM images of the products synthesized under other experimental conditions.

Acknowledgments

The authors thank the financial support from National Key Basic research Program (Grant No. 2002CB211802).

[1] a) X. Wang, J. Zhuang, Q. Peng, Y. D. Li, *Nature* **2005**, *437*, 121–124; b) A. S. Aricò, P. Bruce, B. Scrosati, J. Tarascon, W. V. Schalkwijk, *Nat. Mater.* **2005**, *4*, 366–377; c) X. W. Xie, Y. Li, Z. Q. Liu, M. Haruta, W. J. Shen, *Nature* **2009**, *458*, 746–749.
[2] a) A. Trovarelli, *Catal. Rev. Sci. Eng.* **1996**, *38*, 439–520; b) C. W. Sun, H. Li, L. Q. Chen, *J. Phys. Chem. Solid* **2007**, *68*, 1785–1790.
[3] S. Carrettin, P. Concepcion, A. Corma, J. M. L. Nieto, V. F. Puntes, *Angew. Chem. Int. Ed.* **2004**, *43*, 2538–2540.
[4] a) S. Park, J. M. Vohs, R. J. Gorte, *Nature* **2000**, *404*, 265–267; b) Z. Zhan, S. A. Barnett, *Science* **2005**, *308*, 844–847; c) C. W. Sun, Z. Xie, C. R. Xia, H. Li, L. Q. Chen, *Electrochem. Commun.* **2006**, *8*, 833–838.
[5] H. J. Beie, A. Gnoerich, *Sens. Actuators B* **1991**, *4*, 393–399.

[6] F. Larachi, J. Pierre, A. Adnot, A. Bernis, *Appl. Surf. Sci.* **2002**, *195*, 236–250.
[7] a) Y. M. Chiang, E. B. Lavik, I. Kosacki, H. L. Tuller, *Appl. Phys. Lett.* **1996**, *69*, 185–187; b) C. W. Sun, G. L. Xiao, H. R. Zhang, X. P. Qiu, H. Li, L. Q. Chen, *J. Phys. Chem. B* **2006**, *110*, 13445–13452; c) S. Deshpande, S. Patil, S. Kuchibhatla, S. Seal, *Appl. Phys. Lett.* **2005**, *87*, 133113; d) H. Zhou, Y. Zhang, H. Mai, X. Sun, Q. Liu, W. Song, C. Yan, *Chem. Eur. J.* **2008**, *14*, 3380–3390.
[8] a) M. Yada, S. Sakai, T. Torikai, T. Watari, S. Furuta, H. Katsuki, *Adv. Mater.* **2004**, *16*, 1222–1226; b) C. W. Sun, H. Li, Z. X. Wang, L. Q. Chen, X. J. Huang, *Chem. Lett.* **2004**, *33*, 662–663.
[9] a) S. C. Kuiry, S. D. Patil, S. Deshpande, S. Seal, *J. Phys. Chem. B* **2005**, *109*, 6936–6939; b) A. Vantomme, Z. Y. Yuan, G. Du, B. L. Su, *Langmuir* **2005**, *21*, 1132–1135; c) C. W. Sun, H. Li, H. R. Zhang, Z. X. Wang, L. Q. Chen, *Nanotechnology* **2005**, *16*, 1454–1463.
[10] a) C. Tang, Y. Bando, B. Liu, D. Golberg, *Adv. Mater.* **2005**, *17*, 3005–3009; b) W. Q. Han, L. J. Wu, Y. M. Zhu, *J. Am. Chem. Soc.* **2005**, *127*, 12814–12815; c) K. Zhou, Z. Yang, S. Yang, *Chem. Mater.* **2007**, *19*, 1215–1217; d) G. Chen, C. Xu, X. Song, W. Zhao, Y. Ding, S. Sun, *Inorg. Chem.* **2008**, *47*, 723–728.
[11] a) S. W. Yang, L. Gao, *J. Am. Chem. Soc.* **2006**, *128*, 9330–9331; b) W. I. Hsiao, Y. S. Lin, Y. C. Chen, C. S. Lee, *Chem. Phys. Lett.* **2007**, *441*, 294–299.
[12] a) A. Corma, J. Y. Chane-Ching, M. Airiau, C. Martinez, *J. Catal.* **2004**, *224*, 441–448; b) D. M. Lyons, K. M. Ryan, M. A. Morris, *J. Mater. Chem.* **2002**, *12*, 1207–1212; c) A. K. Sinha, K. Suzuki, *J. Phys. Chem. B* **2005**, *109*, 1708–1714.
[13] R. Si, Y. W. Zhang, S. J. Li, B. X. Lin, C. H. Yan, *J. Phys. Chem. B* **2004**, *108*, 12481–12488.
[14] A. Pfau, K. D. Schierbaum, *Surf. Sci.* **1994**, *321*, 71–80.
[15] C. M. Ho, J. C. Yu, T. Kwong, A. C. Mak, S. Lai, *Chem. Mater.* **2005**, *17*, 4514–4522.
[16] a) A. Trovarelli, *Catalysis by ceria and related materials*, Imperial College Press, London, **2002**, p. 15–50; b) J. A. Wang, J. M. Dominguez, A. Montoya, S. Castillo, J. Navarrete, M. Moran-Pineda, J. Reyes-Gasga, X. Bokhimi, *Chem. Mater.* **2002**, *14*, 4679–4683; c) D. Terribile, A. Trovarelli, C. De Leitenburg, G. Dolcetti, *Chem. Mater.* **1997**, *9*, 2676–2678; d) T. X. T. Sayle, S. C. Parker, C. R. A. Catlow, *Surf. Sci.* **1994**, *316*, 329–336.
[17] Y. N. Xia, P. D. Yang, Y. G. Sun, Y. Y. Wu, B. Mayers, B. Gates, Y. D. Yin, F. Kim, H. Q. Yan, *Adv. Mater.* **2003**, *15*, 353–389.
[18] M. Hirano, E. Kato, *J. Am. Ceram. Soc.* **1999**, *82*, 786–788.
[19] S. Wang, F. Gu, C. Li, H. Cao, *J. Cryst. Growth* **2007**, *307*, 386–394.

Received: April 21, 2009
Published Online: August 7, 2009

